Morphology Change of C_{60} Islands on Organic Crystals Observed by Atomic Force Microscopy

Sara Freund,*,† Antoine Hinaut,† Rémy Pawlak,† Shi-Xia Liu,‡ Silvio Decurtins,‡ Ernst Meyer,† and Thilo Glatzel†

†*Department of Physics, University of Basel, Klingelbergstr. 82, 4056 Basel, Switzerland*

‡*Department of Chemistry and Biochemistry, University of Bern, Freiestr. 3, 3012 Bern, Switzerland.*

E-mail: sara.freund@unibas.ch

Abstract

Organic-organic heterojunctions are nowadays highly regarded materials for light-emitting diodes, field-effect transistors, and photovoltaic cells with the prospect of designing low-cost, flexible, and efficient electronic devices.[1–3] However, the key parameter of optimized heterojunctions relies on the choice of the molecular compounds as well as on the morphology of the organic-organic interface[4] which thus requires fundamental studies. In this work, we investigated the deposition of C_{60} molecules at room temperature on an organic layer compound, the salt bis(benzylammonium)bis(oxalato)-cupurate(II), by means of non-contact atomic force microscopy (nc-AFM). Three-dimensional molecular islands of C_{60} having either triangular or hexagonal shapes are formed on the substrate following a "Volmer-Weber" type of growth. We demonstrate the dynamical reshaping of those C_{60} nano-structures under the local action of the AFM tip at room temperature. The dissipated energy is about 75 meV and can be interpreted as the activation energy required for this migration process.

Keywords: C_{60} molecule, organic compound crystals, manipulation, diffusion, non-contact atomic force microscopy.

Introduction

Within the past years, a large panel of organic/inorganic interfaces has been investigated by means of scanning probe microscopy (SPM), such as organic molecules adsorbed on metals,[5–7] semiconductors[8–11] and insulators.[12–14] However, fundamental studies of organic-organic interfaces are still scarce despite of their great interest for molecular electronic applications.[15]

Transition-metal dicarboxylate complexes enable the formation of two-dimensional anionic layers and are potential candidates as supramolecular building blocks to design organic layered structures.[16–19] The versatility of such materials further offers the possibility to design surfaces with variable chemical end-groups and molecular orientations having thus tunable chemical or mechanical properties. In the salt crystal of bis(benzylammonium)bis(oxalato)-cupurate(II) (BNL), copper oxalate anions $[Cu(C_2O_4)_2]^{2-}$ (Figure 1a) aggregate into planar anionic sheets extended along the [100] and [010] crystallographic directions which are separated by organic benzylammonium cations $(C_6H_5CH_2NH_3)^+$ (Figure 1b).[19] Through hydrogen-ionic bonding between the ammonium groups of the cations and the oxygen atoms of the anions, benzylammonium decorates both sides of the copper oxalate network in a stereoregular way with the benzyl groups in an upright orientation, and slightly tilted to the surface normal leading to an organic and anisotropic surface (Figure 1c). Besides its interesting surface properties, the BNL crystal is known to display intra-layer antiferromagnetic interactions[19] as well as electron-donating properties characterized by a low ionization potential. However, local investigations of this surface remain challenging due to its insulating nature and thus require the use of atomic force microscopy (AFM). So far, Fessler *et al.* reported molecular-scale friction properties measured by means of friction force microscopy (FFM).[20]

Contrarily to the BNL crystal, the fullerene C_{60} has been widely studied in SPM under UHV conditions since its discovery by Kroto *et al.* in 1985.[21] At low temperature, C_{60} molecules were characterized with several SPM techniques on various surfaces and submolecular contrast have been obtained by scanning tunnelling microscopy (STM)[22–24] and non-contact atomic force microscopy (nc-AFM).[25–27] At room temperature (RT), two dimensional C_{60} layers have been observed on metals[28–30] and semiconductors[31–33] while large three dimensional molecular islands or clusters have been revealed on ionic crystals.[34–39] Additionally, the controlled manipulation of C_{60} molecules has also been demonstrated through the action of a SPM tip as single molecules[40–43] or as entire islands.[44]

In the present work, we characterize the adsorption of the C_{60} molecules on the organic lay-

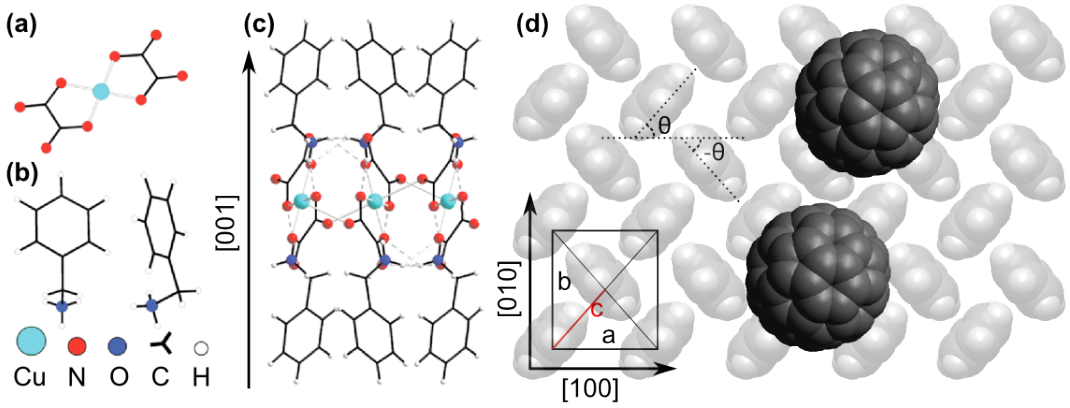

Figure 1: **The Molecular Structure of The BNL Organic Crystal.** **a,** The $[Cu(C_2O_4)_2]^{2-}$ complex extends in a two-dimensional structure which is sandwiched between the organic benzylammonium cations (**b**). **c,** Cross section of the BNL compound. **d,** Two C_{60} molecules adsorbed on the BNL surface. Here the top view of the (001) crystal surface is shown with alternating molecular orientations of the cation. The molecules are rotated by $\theta \simeq \pm 48°$ with respect to the [100] direction. The lattice parameters are $a = 0.71$ nm, $b = 0.80$ nm and $c = 0.53$ nm.[20] The van der Walls diameter of one C_{60} molecule is ~ 1 nm and is close to $2c$.

ered crystal, BNL. The van der Waals radius of the C_{60} corresponds to the distance between two benzylammonium rows with opposite molecular orientations (Figure 1d). Due to the high electron affinity of the C_{60},[45] it is considered to be an interesting candidate to build an organic-organic interface on the electron-donor BNL surface.

Results and Discussion

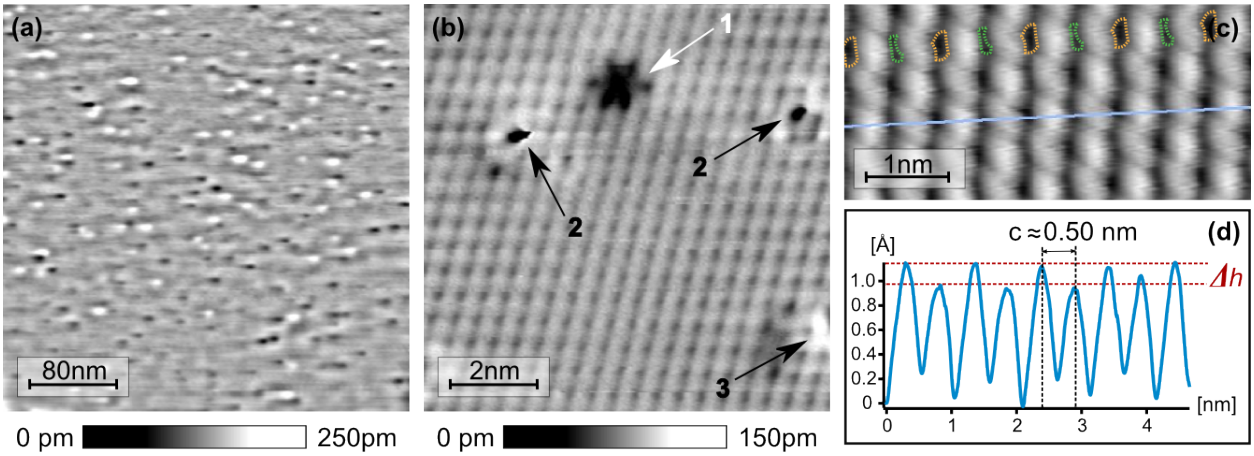

Figure 2: **Topographic nc-AFM Images of The BNL Surface. a,** Topographic image of the BNL crystal presenting a flat surface covered with defects. **b,** High-resolution topographic image showing several types of defects. **c,** High-resolution topographic image of a defect-free area. **d,** Profile acquired along the light blue line visible in **c**. Two different molecular orientations are visible and the spacing between the molecules corresponds to the expected lattice parameter of BNL. Scan parameters: (a) $A_{f_1} = 4$ nm, $\Delta f_1 = -9$ Hz; (b) $A_{f_1} = 2$ nm, $\Delta f_1 = -8$ Hz; (c) $A_{f_1} = 5$ nm, $\Delta f_1 = -75$ Hz.

Atomic-Resolution on The BNL Organic Crystal. Figure 2 shows nc-AFM images of the BNL at the atomic scale. The surface of the crystal is atomically flat over several hundreds of nanometers. The large scale topographic image Figure 2a presents a terrace of 400×400 nm^2 without step edges. The crystal is covered with low-height or shallow defects (ΔZ = 250 pm) with an average roughness of R_a = 35.8 pm.

These defects are highlighted in the zoom in topographic image on the BNL substrate (Figure 2b) obtained with molecular resolution. Two types of defects are indicated in Figure 2b with black and white arrows. The white arrow shows a star-like vacancy (type 1) due to two missing molecules. The black arrows indicate other types of defects which are either stretched (type 2) or buckled (type 3), which we think result from sub-surface defects such as misoriented molecules in lower layers.

Figure 2c displays a highly resolved nc-AFM image of a defect-free area of the BNL surface. The distance between two molecules is approximatively 0.50 nm and coincides with the expected value of the BNL lattice parameters (c $\simeq$ 0.53 nm in Figure 1d). Similar to previous friction measurements,[20] the image reveals two different molecular orientations at the surface corresponding to the alternating height difference of the molecular rows as shown in the profile (Figure 2d) measured along the light blue line in Figure 2c. The alternating shape of the corrugations between the rows (shown in orange and green) corresponds to two different alternating molecular orientations.

C_{60} Adsorbed on BNL. Upon C_{60} deposition, molecules form molecular islands on BNL at RT, as shown on the large scale topographic image (Figure 3a). Isolated molecules or smaller clusters were never observed, neither at lower coverage rate nor on small defects or step edges. Furthermore, we noticed that the defects observed on the BNL surface, seem not to act as preferentially adsorption sites for the C_{60} molecules. Indeed, the average distance between the island is not the same than the average distance between the defects.

The average distance between islands is approximatively 45 nm. This relatively large distance suggests that the molecules easily diffuse on the BNL substrate, implying that they are rather weakly coupled to the surface. This behaviour is similar to C_{60} adsorbed on ionic crystals.[34–39,44] However, in contrast to C_{60}/ionic crystals, C_{60} islands on BNL extend rather in height than in width (approximately 10 times narrower than on ionic crystals). Therefore, the growth is governed by a "Volmer-Weber-like" growth mode and suggests a weaker molecule/surface interaction on BNL than on bulk insulators.

Two different shapes of the C_{60} island are observed which, in both cases, present 6 edges. In the first configuration, the island has almost equal edges whereas the second configuration presents three long and three short ones. For clarity purposes, we will refer in the following work to them as "hexagonal" and "triangular" islands, respectively. The population ratio of triangular versus hexagonal islands is close to 1:1 and is stable against ageing (Figure 3a). Indeed, we observed other areas of the same sample several weeks after deposition, always re-

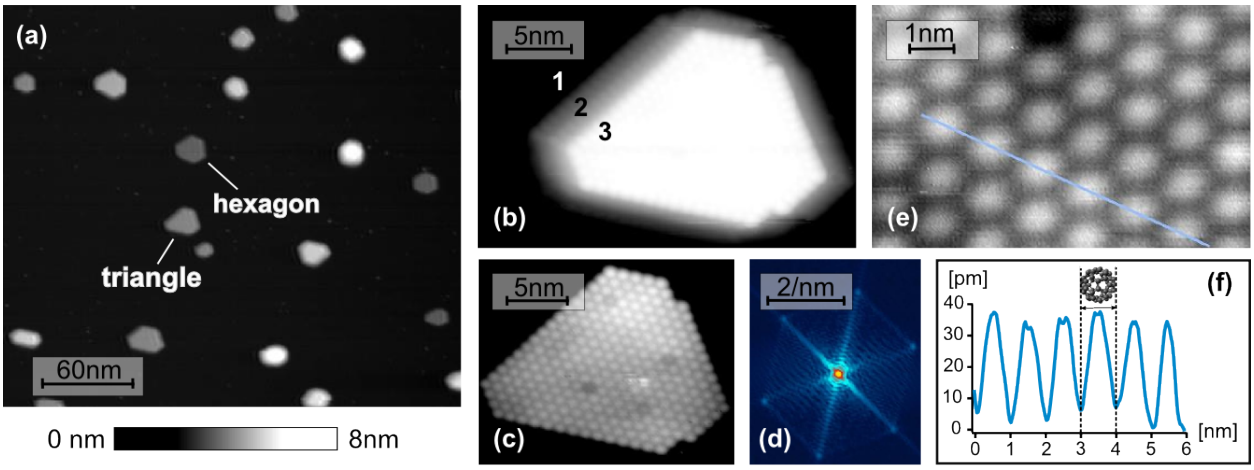

Figure 3: **High Resolution Imaging Of a C_{60} Island.** (**a,**) Topographic image of the C_{60} islands on the BNL substrate. (**b,**) Triangular island formed of three monolayers and (**c,**) is a topographic image of the upper layer of the C_{60} islands shown in (**b**). The fast Fourier transform (FFT) (**d**) was calculated on (**c**) and highlights an hexagonal packing of the C_{60} molecules. The profile (**f**) was extracted along the blue line in (**e**) and confirms the values of the surface lattice parameters measured on the FFT: $a \simeq b \simeq c \simeq 1$ nm. Scan parameters: (a-e) $A_{f_1} = 2$ nm, $\Delta f_1 = -30$ Hz.

vealing similar proportion. Both configurations are thus stable at RT and the energy needed to turn one shape into the other is not accessible by this temperature.

Figure 3b shows a triangular-shaped island which consists of three C_{60} layers (total height is 3 nm). The contrast of this image was further enhanced to observe the upper layer with molecular resolution (Figure 3c) and the darker spots correspond to C_{60} vacancies. The fast fourier transform (FFT) (Figure 3d) extracted from the image Figure 3c shows the lattice parameter of the C_{60} hexagonal packing. The profile of Figure 3f highlights the distance between the molecules which corresponds to the lattice parameter expected for bulk C_{60} ($a \simeq b \simeq 1$ nm). Since the top layer of the island was unambiguously observed with molecular resolution, we extracted the density of C_{60} to ~ 1.4 molecules/nm^2.[46] Knowing the island height, we further calculated the number of molecules per island depending on its size and shape. For the triangular island represented in Figure 3(b), this number was estimated to ~ 1285 molecules.

Tip-Induced Manipulations. Island shape modification is a phenomenon which was

already reported in previous works.[37–39,47–49] The process is due to the tendency of molecules to aggregate in 2D or 3D fashion in order to optimize the surface energy, which is a subtle balance between molecule/surface and molecule/molecule interactions. Shape modifications can be triggered by thermodynamic effects such as temperature changes[48] or by the local action of a SPM tip continuously scanning the island.[49]

Figure 4 shows such tip-induced modification of the C_{60} island morphology. During the process, a triangular island (Figs. 4a) was turned into a hexagonal island (Figure4b). The shape modification process was initiated at close tip-sample distance by decreasing the scan setpoint of approximatively 65% compared to standard conditions employed in Figs. 4a and b. These large scale images were indeed recorded with larger tip-sample separations (typical $\Delta f_1 \approx$ -30 Hz) to ensure stable imaging conditions whereas all the images in Figs. 4d-h were recorded at lower setpoints varying from -60 Hz $\leq \Delta f_1 \leq -47$ Hz. The whole sequence of images was acquired in the blue area marked in Figs. 4a and b and reveals the change of the island morphology. Figure 4f particularly points out the building up of a new monolayer above the already existing ones. We observe that the C_{60} molecules travelled from the edges of the island to its top to form this fourth monolayer. The profile of the shape evolution, displayed on Figure 4c, confirms the formation of a new C_{60} monolayer since the height of the island increased from 3 to 4 nm (*i.e.* from three to four layers). Figures 4a and b were recorded before and after the island underwent its shape modification process, respectively. The comparison of these two pictures indicates that the shape evolution is tip-induced because only the island of the blue area clearly modified its shape. Other significant shape changes were not observed for neighbouring islands during this time.

Thanks to high resolution imaging, the number of the molecules which composes the C_{60} island is estimated from Figs. 4d and f to $\sim$ 1362 molecules for the triangular island (Figure 4d) and $\sim$ 1386 molecules for the hexagonal (Figure 4f). This corresponds to a difference of 24 molecules, *i.e.* an error of $\sim$ 1.7%, and corroborates the assumption that molecules forming the fourth layer of the hexagonal island are moved from the edges of

the triangular island to its top. The contact area of the island, which corresponds to the area of the first layer obtained from AFM measurements, varies from $\sim$ 410 nm^2 for the triangle to $\sim$ 356 nm^2 for the hexagon, *i.e.* a reduction of $\sim$ 14%. This confirms that the molecule/molecule interaction is favoured whereas the molecule/substrate interaction is minimized upon shape modification, which is in agreement with the "Volmer-Weber" type of growth. Assuming that the interaction energy between two C_{60} molecules is $E_i \sim 130$ meV[50] and neglecting their interactions with the BNL substrate, we estimate the cohesion energy (E_C) of the island before and after it undergoes the shape-modification process by summing the interactions energies of all C_{60} with their nearest neighbours in or out of plane. The cohesion energies of the triangular and hexagonal islands are estimated to 484 meV/molecule and 495 meV/molecule, respectively. Thus, the triangular island is lower in energy ($\sim$ 11 meV/molecules) than the hexagonal island implying that the first configuration is less stable than the second ($\sim$ 2.25%).

To support the experimental data, we considered two perfect island shapes, which consist of a three monolayer-high triangular island with truncated vertexes and a four monolayer-high hexagonal island (Figure 5b and d). The triangle and the hexagon are composed of 1387 and 1388 molecules, respectively, which correspond to an error of $\sim$ 0.07%. The contact areas of the two islands were estimated to $\sim$ 436 nm^2 for the triangular island and $\sim$ 380 nm^2 for the hexagonal island, which is in agreement with the experimental data. In this ideal case, the contact area decreases by $\sim$ 13% during the shape modification process. The cohesion energies are also estimated to 491 meV/molecule and 506 meV/molecule for the ideal triangular- and the hexagonal-shaped island, respectively; *i.e.* a difference of 15 meV/molecules. Table 1 resumes these values extracted from the experiments and this model.

Based on this observation, we conclude that the hexagonal shape is definitely more stable than the triangular configuration since it favours molecule/molecule interactions. Importantly, the tip-induced shape modification experiment was performed eleven days after

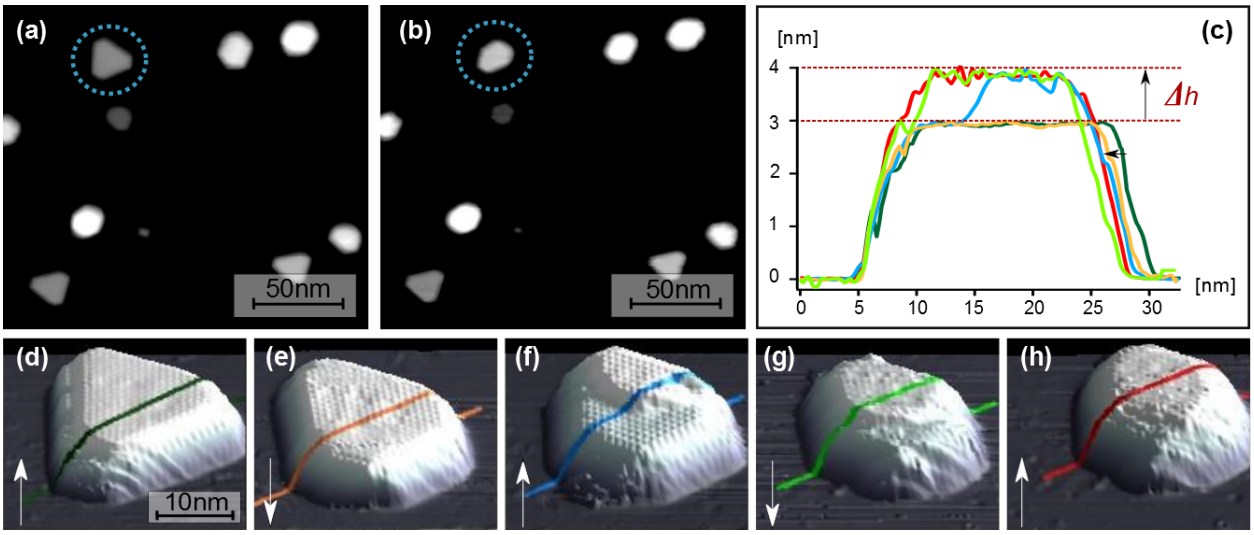

Figure 4: **Tip-Induced Shape Modification of a C_{60} Island. a-b,** are topographic images recorded before and after the tip-induced shape modification process, respectively, $\Delta f_1 = -31$ Hz. **c,** Profiles of the C_{60} island acquired while modifying its shape from triangular to hexagonal. **d-h,** Sequence showing the shape modification process. The tip was continuously scanned over the island but the tip/sample distance was intentionally varied by changing Δf_1 to scan the island. Slow scan directions are given by the white arrows. Scan parameters: $A_{f_1} = 2$ nm; (a-b) $\Delta f_1 = -31$ Hz; (d) $\Delta f_1 = -46$ Hz; (e) $\Delta f_1 = -51$ Hz; (f) $\Delta f_1 = -60$ Hz; (g) $\Delta f_1 = -55$ Hz; (h) $\Delta f_1 = -55$ Hz.

Table 1: Summary of The Experimental And Model Values

Shape	Number of molecules/island		Contact area $[nm^2]$		Cohesion energy $[meV/molecule]$	
	Exp.	Model	Exp.	Model	Exp.	Model
△	1362	1387	410	436	484	491
⬡	1386	1388	352	380	495	506
$\lvert\triangle - \hexagon\rvert$	24	1	58	56	11	15

the C_{60} molecules were evaporated on the BNL. This time interval is normally long enough for the islands to undergo thermally induced morphology changes. Since both structures are still present after such time (Figure 4a), we assume that the transition from triangular to hexagonal phases requires to overcome an energy barrier which is higher than the energy accessible at RT. Assuming an Arhenius-like energy pathway as depicted in Figure 5e, the local perturbation of the AFM tip allows the activation of the transition between triangle and hexagon. In order to estimate such activation energy, we extracted the dissipated energy by the cantilever during the morphological evolution of the molecular island presented

in Figure 4 with the formula :

$$E_A \approx E_0 \left(\frac{A_{exc}}{A_{exc,0}} - 1 \right) \tag{1}$$

where $E_0 = \pi k A^2/Q$ is the intrinsic loss energy, A_{exc} is the drive amplitude to keep a certain oscillation amplitude and $A_{exc,0}$ is the drive amplitude far from the surface .[51,52] The values for A_{exc} were extracted from the dissipation images obtained experimentally. In order to do so, we first identified, in the topographic images, the areas where we noticed a clear modification of the island morphology (which is characterized by curved edges for instance). We then extracted about 60 drive amplitudes per images and averaged them to obtain a value for A_{exc}. $A_{exc} \simeq 4.65$ mV with a deviation of $\sigma \simeq 1$ mV. The dissipated energy is thus calculated to be ~ 75 meV per oscillation cycle during the change of morphology. This energy E_A is slightly higher than the excitation energy accessible at RT ($kT \simeq 30$ meV), which supports the fact that the transition from triangle to hexagonal phases cannot occur spontaneously at RT. Note also that the diffusion of the C_{60} on the BNL surface is possible at RT according to the AFM data since a spontaneous formation of two metastable island configurations is observed on BNL (diffusion energy: $E_{d(C_{60}/BNL)} < kT$). Additionally, we think that E_A, which is the activation energy required to reshape the hexagonal island, can be considered as corresponding to two effects: the crossing of the Ehrlich-Schwoebel barrier (E_{ES}; which is the energy required for a C_{60} to cross the potential well at the step edge) [53,54] and the diffusion of the C_{60} on the island ($E_{d(C_{60}/C_{60})}$) (Figure 5(f)). Recently, these values have been reported by combining numerical simulation and real-time X-ray scattering[50] and are in good agreement with our experiments.

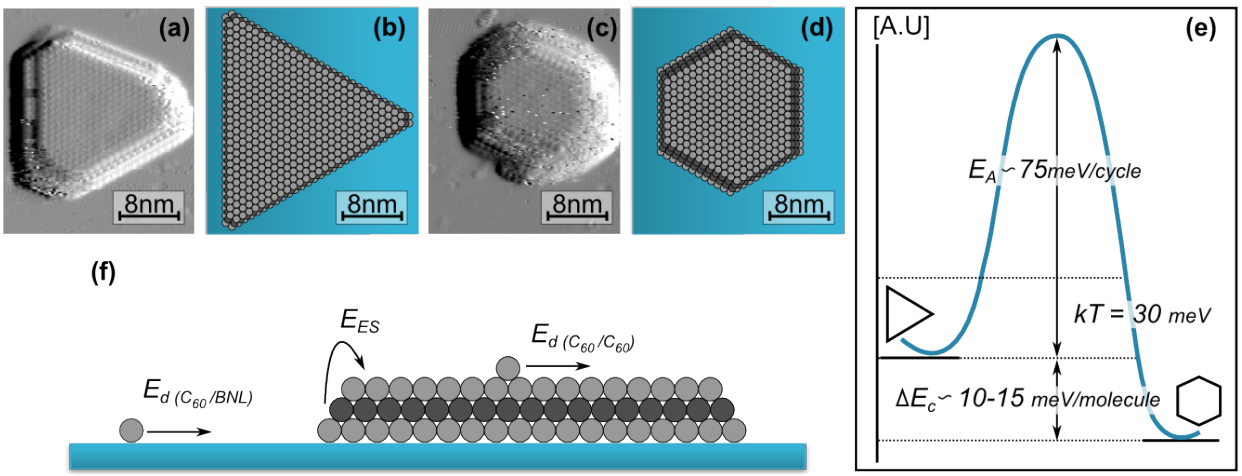

Figure 5: **Model For Triangular- And Hexagonal-Shaped Islands. a-c,** Derivative of topography AFM images recorded on the same island before and after it the morphology change, respectively. **b,** A simple model shows that a three monolayer high triangular island can be turned in a four monolayer high hexagonal island by reshaping its structure **d**. **e,** The triangular island is less stable than the hexagonal island according to the model and experiments. Their cohesion energies (E_C) are calculated to be 491 meV/molecule and 506 meV/molecule, respectively. E_A represents the activation energy needed to turn the triangular- into an hexagonal island. **f,** The diffusion energy of C_{60} on BNL $E_{d(C_{60}/BNL)}$ is $< kT$, whereas the Ehrlich-Schwoebel barrier energy are $E_{ES} = E_A \simeq 75$ meV and the diffusion energy of the C_{60} on the island is $kT \leqslant E_{d(C_{60}/C_{60})} \leqslant E_A$.

Conclusion

We presented herein high-resolution topographic images using nc-AFM at room temperature of C_{60} molecules adsorbed on the surface of the BNL crystal. The surface structure of BNL was resolved with molecular precision and the two expected molecular orientations of the benzylammonium structure are observed at the crystal surface. Large scale images show that few defects are also present at this surface. Upon C_{60} deposition, molecules form islands at room temperature on the BNL substrate having either hexagonal or triangular shapes. We demonstrated the capability to locally induce a change of the island morphology via the action of the AFM tip. A simple model suggests that the triangular domains are slightly less energetically favorable than the hexagonal ones. The reshaping process is obtained by dissipating energy ($\sim$ 75 meV) from the cantilever to the islands which corresponds to the Ehrlich-Schwoebel barrier of C_{60} layers as well as the diffusion energy of C_{60} on C_{60}

layers. Such results open the way for the local study of further organic-organic interfaces with variable functionalities and notably a better understanding of their growth properties at the atomic scale.

Method

Sample Preparation. The BNL crystals used in this study were synthesized at the University of Bern by Decurtins *et al.* according to the literature method.[19] These thin light blue crystals were glued with the electrical conductive Epotek H20S glue on a previously modified standard metallic sample holder and were heated up to 100° C for 1h in air. Thereafter, the surface was exfoliated with a scotch tape and quickly introduced in vacuum resulting in an atomically clean and flat surface. A C_{60} powder with purity of 99.9%, purchased from Sigma Aldrich GmbH, was evaporated at 410° C on the BNL surface at room temperature under UHV conditions. The deposition time was fixed to 30 sec with a deposition rate of 0.5 $\mathring{A}$/min. This deposition rate was calibrated by a quartz microbalance.

Scanning Probe Microscopy. The SPM measurements were realized with a home built UHV RT-AFM microscope. All AFM images were recorded in the non-contact mode, using silicon tips (stiffness of k = 20-30 N/m, resonance frequency f_0 around 155 kHz and Q factor around 30000) with compensated contact potential difference (CPD). The bias voltage applied to the tip-sample system was $-10V \leq V_{bias} \leq 10V$.

Energy Calculation. The cohesion energy (E_C) of the island before and after it undergoes the shape-modification process was estimated with the formula:

$$E_C = \frac{1}{n_{total}} \cdot \frac{E_i}{2} \left[\sum_{\substack{k=3,4,6 \\ intra-layer}} k \cdot n_k + \sum_{\substack{k=3 \\ inter-layer}} k \cdot n_k \right] \tag{2}$$

where n_{total} is the total number of molecules in the island, E_i the interaction energy between two molecules, k the number of first nearest neighbours and n_k is the number of C_{60} with k nearest neighbours.

Acknowledgements

This work was supported by the Swiss National Science Foundation (SNF), Polish-Swiss Project PSPB-085/2010, the Swiss Nanoscience Institute (SNI) and the COST Action MP1303.

Competing Financial Interests statement

The authors declare no competing financial interests.

References

(1) Tang, C.W.; VanSlyke, S. A. Organic Electroluminescent Diodes. *Appl. Phys. Lett.* **1987** *51,* 913–915.

(2) Garnier, F.; Hajlaoui, R.; Yassar, A.; Srivastava, P. All-Polymer Field-Effect Transistor Realized by Printing Techniques. *Science* **1994,** *265*, 1684-1686.

(3) Tang; C. W. Two-Layer Organic Photovoltaic Cell. *Appl. Phys. Lett.* **1986,** *86,* 183-185.

(4) Koch, N. Organic Electronic Devices And Their Functional Interfaces. *Chem. Phys. Chem.* **2007,** *8,* 1438–1455.

(5) Gotsmann, B.; Schmidt, C.; Seidel, C.; Fuchs, H. Molecular Resolution of An Organic Monolayer by Dynamic AFM. *Eur. Phys. J. B* **1998,** *4,* 267–268.

(6) Lukas, S.; Witte, G.; Wöll, Ch. Novel Mechanism For Molecular Self-Asssembly

on Metal Substrate: Unidirectional Rows of Pentacene on Cu(110) Produced by a Substrate-Mediated Repulsion. *Phys. Rev. Lett.* **2001,** *88*, 028301.

(7) Zambelli, T.; Tang, H.; Lagoute, J.; Gourdon, A.; Joachim, C. Conformations of a Long Molecular Wire With Legs on a Cu(100) Surface. *Chem. Phys. Lett.* **2001, 348,** 1–6.

(8) Li, L.; Tindall, C.; Takoaka, O.; Hasegawa, Y.; Sukarai, T. STM Study of C_2H_2 Adsorption on Si(001). *Phys. Rev. B* **1997,** *56,* 4648–4655.

(9) Hamers, R. J.; Hovis, J. O.; Lee, S.; Liu, H.; Shan, J. Formation of Ordered, Anisotropic Organic Monolayers on The Si(001) Surface. *J. Phys Chem. B* **1997,** *101,* 1489–1492.

(10) Sasahara, A.; Uetsuka, H.; Onishi, H. NC-AFM Topography of HCOO And CH_3COO Molecules Co-Adsorbed on TiO_2(110). *Appl. Phys. A* **2001,** *72,* S101–S103.

(11) Schütte, J.; Bechstein, R.; Rahe, P.; Rohlfing, M.; Künhle, A.; Langhals, H. Imaging Perylene Derivatives on Rutile TiO_2(110) by Noncontact Atomic Force Microscopy. *Phys. Rev. B* **2009,** *79,* 045428.

(12) Nony, L.; Gnecco, E.; Baratoff, A.; Alkauskas, A.; Bennewitz, R.; Pfeiffer, O.; Maier, S.; Wetzel, A.; Meyer, E.; Gerber, Ch. Observation of Invidual Molecules Trapped on a Nanostructured Insulator. *Nano Lett.* **2004,** *4,* 2185–2189.

(13) Kunstmann, T.; Schlarb, A.; Fendrich, M.; Wagner, Th.; Möller, R.; Hoffmann, R. Dynamic Force Microscopy Study of 3,4,9,10-Perylenetetracarboxylic Dianhydride on KBr(001). *Phys. Rev. B* **2005,** *71*, 121403(R).

(14) Topple,, J. M.; Burke, S. A.; Ji, W.; Fostner, S.; Tekiel, A.; Grütter, P. Tailoring The Morphology And Dewetting of an Organic Thin Film. *J. Phys. Chem. C* **2011,** *115,*, 217–224.

(15) Aviram, A.; Ratner, M. A. Molecular Rectifiers. *Chem. Phys. Lett.* **1974,** *29,* 277–283.

(16) Clément, R.; Decurtins, S.; Gruselle, M.; Train, C. Polyfunctional Two- (2D) and Three- (3D) Dimensional Oxalate Bridged Bimetallic Magnets. *Monatsh. Chem.* **2003,** *134*, 117–135.

(17) Gruselle, M.; Train, C.; Boubekeur, K.; Gredin, P.; Ovanesyan, N. Enantioselective Self-Assembly of Chiral Bimetallic Oxalate-Based Networks. *Coordin. Chem. Rev.* **2006,** *250*, 2491–2500.

(18) Keene, T. D.; Zimmermann, I.; Neels, A.; Sereda, O.; Hauser, J.; Liu, S.-H.; Decurtins, S. Crystal Engineering of a Series of Arylammonium Copper(II) Malonates. *Cryst. Growth Des.* **2010,** *10*, 1854–1859.

(19) Bloomquist, D. R.; Hansen, J. J.; Landee, C. P.; Willett, R. D.; Buder, R. Structure And Magnetic Properties of Two Two-Dimensional Copper Oxalates: Bis(Benzylammonium) Bis(Oxalato)Cuprate(II) And Propylenediammonium Bis(Oxalato)Cuprate(II.) *Inorg. Chem.* **1981; 20,** 3308–3314.

(20) Fessler, G.; Zimmermann, I.; Glatzel, T.; Gnecco, E.; Steiner, P.; Roth, R.; Keene, T. D.; Liu, S.-X., Decurtins, S.; Meyer, E. Orientation Dependent Molecular Friction on Organic Layer Compound Crystals. *Appl. Phys. Lett.* **2011,** *98*, 083119.

(21) Kroto, H. W.; Heath, J. R.; O'Brien, S. C.; Curl, R. F.; Smalley, R. E. C_{60}: Buckminsterfullerene. *Chem. Rev.* **1985,** *91,* 1213–1235.

(22) Lu, X.; Grobis, M.; Khoo, K. H.; Louie, S. G.; Crommie, M. F. Charge Transfer And Screening in Individual C_{60} Molecules on Metal Substrates: A Scanning Tunneling Spectroscopy And Theoretical Study. *Phys. Rev. B* **2004,** *70*, 115418.

(23) Schull, G.; Néel, N.; Becker, M.; Kröger, J.; Berndt, R. Spatially Resolved Conductance of Oriented C_{60}. *New J. Phys.* **2008,** *10,* 065012.

(24) Samuely, T.; Liu, S.-X.; Haas, M.; Decurtins, S.; Jung, T. A.; Stöhr, M. Self-Assembly of Individually Addressable Complexes of C_{60} And Phthalocyanines on a Metal Surface: Structural And Electronic Investigations. *J. Phys. Chem. C* **2009,** *113,* 19373–19375.

(25) Pawlak, R.; Kawai, S.; Fremy, S.; Glatzel, T.; Meyer, E. Atomic-Scale Mechanical Properties of Orientated C_{60} Molecules Revealed by Non-Contact Atomic Force Microscopy. *ACS Nano* **2011,** *5,* 6349–6352.

(26) Pawlak, R. ; Kawai, S.; Fremy, S.; Glatzel, T.; Meyer, E. High-Resolution Imaging of C_{60} Molecules Using Tuning-Fork-Based Non-Contact Atomic Force Microscopy. *J. Phys. - Condens. Mat.* **2012,** *24,* 084005.

(27) Gross, L.; Mohn, F.; Moll, N.; Schuler, B.; Criado, A.; Guitián, E.; Peña, D.; Gourdon, A.; Meyer, G. Bond-Order Discrimination by Atomic Force Microscopy. *Science* **2012,** *337,* 1326–1329.

(28) Mativetsky, J. M.; Burke, S. A.; Hoffmann, R.; Sun, Y.; Grütter, P. Molecular Resolution Imaging of C_{60} on Au(111) by Non-Contact Atomic Force Microscopy. *Nanotechnology* **2004,** *15,* S40.

(29) Altman, E. I.; Colton, R. J. Determination of The Orientation of C_{60} Adsorbed on Au(111) And Ag(111). *Phys. Rev. B* **1993,** *48,* 18244–19249.

(30) Hashizume, T.; Mota, K.; Wang, X. D.; Shinohara, H.; Saito, Y.; Maruyama, Y.; Ohno, K.; Kawazoe, Y.; Nishina, Y.; Pickering, H. W. *et al.* Intramolecular Structures of C_{60} Molecules Adsorbed on The Cu(111)-(1×1) Surface. *Phys. Rev. Lett.* **1993,** *71,* 2959–2962.

(31) Loske, F.; Bechstein, R.; Schütte, J.; Ostendorf, F.; Reichling, M.; Kühnle, A. Growth of Ordered C_{60} Islands on TiO_2(110). *Nanotechnology* **2009,** *20,* 065606.

(32) Kobayashi, H.; Yamada; H.; Horiuchi, T.; Matsushige, K. Investigations of C_{60} Molecules Deposited on Si(111) by Noncontact Atomic Force Microscopy. *Appl. Surf. Sci.* **1999,** *140,* 281–286.

(33) Sanvitto, D.; De Seta, M.; Evangelisti, F. Growth of Thin C_{60} Films on Hydrogenated Si(100) Surfaces. *Surf. Sci.* **2000,** *452,* 191–197.

(34) Loske, F.; Lübbe, J.; Schütte, J.; Reichling, M.; Kühnle, A. Quantitative Description of C_{60} Diffusion on An Insulating Surface. *Phys. Rev. B* **2010,** *82,* 155428.

(35) Loske, F.; Reichling, M.; Kühnle, A. Steering Molecular Island Morphology On An Insulator Surface by Exploiting Sequential Deposition. *Chem. Commun.* **2011,** *47,* 10386–10388.

(36) Burke, S.; Mativetsky, M.; Hoffmann, R.; Grütter, P. Nucleation And Submonolayer Growth of C_{60} on KBr. *Phys. Rev. Lett.* **2005,** *94,* 096102.

(37) Burke, S.; Topple, J. M.; Grütter, P. Molecular Dewetting on Insulators. *J. Phys. - Condens. Mat.* **2009,** *21*, 423101.

(38) Burke, S.; Mativetsky, M.; Fostner, S.; Grütter, P. C_{60} on Alkali Halides: Epitaxy And Morphology Studied by Noncontact AFM. *Phys. Rev. B* **2007,** *76,* 035419.

(39) Körner, M.; Loske, F.; Einax, M.; Kühnle, A.; Reichling, M.; Maass, P. Second-Layer Induced Island Morphologies in Thin-Film Growth of Fullerenes. *Phys. Rev. Lett.* **2011,** *107,* 016101.

(40) Loske, F.; Kühnle A. Manipulation of C_{60} Islands on The Rutile TiO_2 (110) Surface Using Noncontact Atomic Force Microscopy. *Appl. Phys. Lett.* **95**, 043110 (2009).

(41) Beton, P. H.; Dunn, A. W.; Moriarty, P. Manipulation of C_{60} Molecules on a Si Surface. *Appl. Phys. Lett.* **1995,** *67,* 1075–1077.

(42) Cuberes, M. T.; Schlittler, R. R.; Gimzewski, J. K. Room Temperature Repositioning of Individual C_{60} Molecules at Cu Steps: Operation of a Molecular Counting Device. *Appl. Phys. Lett.* **1996,** *69,* 3016–3018.

(43) Dunn, A. W.; Beton, P. H.; Moriarty, P. C_{60} Manipulation And Cluster Formation Using a Scanning Tunneling Microscope. *J. Vac. Sci. Technol. B* **1996,** *14,* 1596–1599.

(44) Lüthi, R.; Meyer, E.; Haefke, H.; Howald, L.; Gutmannsbauer, W.; Güntherodt, H. J. Sled-Type Motion on the Nanometer Scale: Determination of Dissipation and Cohesive Energies of C_{60}. *Science* **1994,** *266,* 1979–1981.

(45) Beljonne, D.; Cornil, J.; Muccioli, L.; Zannoni, C.; Brédas, J. L.; Castet, F. Electronic Processes at Organic-Organic Interfaces: Insight From Modeling And Implications For Opto-Electronic Devices. *Chem. Mater.* **2011,** *23,* 591–609.

(46) Horcas, I.; Fernández, R. ; Gómez-Rodríguez, J. M.; Colchero, J.; Gómez-Herrero, J.; Baro, A. M. WSXM: A Software For Scanning Probe Microscopy And a Tool For Nanotechnology. *Rev. Sci. Instrum.* **2007,** *78,* 013705.

(47) Burke, S.; Ji, W.; Mativetsky, J. M.; Topple, J. M.; Fostner, S.; Gao, H.-J.; Guo, H. ; Grütter, P. Strain Induced Dewetting of a Molecular System: Bimodal Growth of PTCDA on NaCl. *Phys. Rev. Lett.* **2008,** *100,* 186104.

(48) Gruznev, D. V.; Matetskiy, A. V.; Bondarenko, L. V.; Utas, O. A.; Zotov, A. V.; Saranin, A. A.; Chou, J. P.; Wei, C. M.; Lai, M. Y.; Wang, Y. L. Stepwise Self-Assembly of C_{60} Mediated by Atomic Scale Moire Magnifiers. *Nature Comm.* **203,** *4,* 1679.

(49) Zebari, A. A. A.; Kolmer, M.; Prauzner-Bechcicki, J. S. STM Tip-Assisted Engineering of Molecular Nanostructures: PTCDA Islands on Ge(001):H Surfaces. *Beilstein J. Nanotechnol.* **2013,** *4,* 927–932.

(50) Bommel, S.; Kleppmann, N.; Weber, C.; Spranger, H.; Schäfer, P.; Novak, J.; Roth S. V.; Schreiber, F.; Klapp, S. H.; Kowarik, S. Unravelling The Multilayer Growth of The Fullerene C_{60} in Real Time. *Nat. Commun.* **2014,** *5,* 1–8.

(51) Anczykowski, B.; Gotsmann, B.; Fuchs, H.; Cleveland, J. P.; Elings, V. B. How To Measure Energy Dissipation in Dynamic Mode Atomic Force Microscopy *Appl. Surf. Sci.* **1999,** *140,* 376.

(52) Kawai, S.; Glatzel, T.; Such, B.; Koch, S.; Baratoff, A.; Meyer, E. Energy Dissipation in Dynamic Force Microscopy on KBr(001) Correlated With Atomic-Scale Adhesion Phenomena. *Phys. Rev. B* **2012,** *86,* 245419.

(53) Ehrlich, G. ; Hudda, F. G. Atomic View of Surface Self-Diffusion: Tungsten on Tungsten. *J. Chem. Phys.* **1996,** *44,* 1039–1049.

(54) Schwoebel, R. L.; Shipsey, E. J. Step Motion on Crystal Surfaces. *J. Appl. Phys.* **1966,** *37,* 3682–3686).